ETH zürich

ETH Library

Control of a III-V MOCVD Process using Ultraviolet Absorption and Ultrasonic Concentration Monitoring

Journal Article

Author(s):
Gaffney Flynn, Monique; Smith, Roy; Abraham, Patrick; DenBaars, Steven P.

Publication date:
2001-09

Permanent link:
https://doi.org/10.3929/ethz-b-000672258

Rights / license:
In Copyright - Non-Commercial Use Permitted

Originally published in:
IEEE Transactions on Control Systems Technology 9(5), https://doi.org/10.1109/87.944468

This page was generated automatically upon download from the ETH Zurich Research Collection.
For more information, please consult the Terms of use.

Published: *IEEE Trans. Control Systems Technology,* vol. 9, no. 5, pp. 728–740, Sept. 2001. doi: 10.1109/87.944468

Control of a III-V MOCVD Process using Ultraviolet Absorption and Ultrasonic Concentration Monitoring

Monique Gaffney Flynn, Roy Smith, Patrick Abraham, Steven DenBaars

***Abstract*—Metalorganic chemical vapor deposition (MOCVD) is a key technology for the growth of compound semiconductors. This process has traditionally lacked real-time growth monitoring and control, which limits the precise reproducibility needed for high performance devices. Two complementary control approaches for the MOCVD process are investigated experimentally. The first is a feedforward disturbance rejection strategy using ultrasonic concentration measurements to reject source gas bubbler disturbances. The second is a feedback system using an ultraviolet (UV) absorption sensor for real-time monitoring of reaction chamber gas concentrations. Post-growth X-ray diffraction and photoluminescence of InP/GaInAs superlattice test devices are used to evaluate control system performance.**

***Index Terms*—Ultrasonic concentration monitor, Ultraviolet absorption, Compound semiconductor, Process control, Semiconductor manufacturing**

I. Introduction

In the past few years, metalorganic chemical vapor deposition (MOCVD) has emerged as one of the most promising techniques for production of the next generation of high speed electronic and opto-electronic devices. However, the industrial application of MOCVD techniques currently suffer from a lack of *in situ* process control, which causes a lack of precise reproducibility. Stricter semiconductor device tolerance requirements are driving the need for better monitoring and control in semiconductor fabrication processes. Device applications such as distributed Bragg reflectors, microcavity LEDs, high mobility layer devices, and heterojunction bipolar transistors require the ability to control composition and layer thickness to high accuracy. The precision can be improved by applying feedforward and feedback control strategies to the MOCVD process and this is the focus of our paper. The major difficulties in controlling this process are technological and include: sensor and actuator selection, process modeling, sensor development and characterization, and control motivated reactor design modifications.

This work was supported by NSF (under grants ECS–9308917, ECS–900047, and ECS–9634498), DARPA (under DURIP grant DAAH–95–1–0061), the ARPA funded Optoelectronics Technology Center at UCSB, the Ralph M. Parsons Foundation, the UCSB Graduate Division, and the UC Office of the President.

M.G. Flynn is with Litton Guidance and Control Systems, Goleta, CA.

R. Smith (corresponding author: roy@ece.ucsb.edu) is with the Electrical and Computer Engineering Department, University of California, Santa Barbara, CA 93106.

P. Abraham is with Agility Communications, Santa Barbara, CA.

S. DenBaars is with both the Materials Department and the Electrical and Computer Engineering Department, University of California, Santa Barbara.

The growth of compound semiconductors requires that the epitaxial layers be of a single-crystalline nature and uniform composition. The introductory work in feedback control of compound semiconductor growth used an organometallic molecular beam epitaxy process and is found in [1]. Growth rate sensing used a spectroscopic ellipsometer, capable of measurements over a band of wavelengths. Post-growth composition evaluation was performed by secondary-ion mass spectrometry. Further work on growth rate and composition control of aluminum gallium arsenide ($Al_xGa_{(1-x)}As$) quantum-well laser structures is described in [2]. The control actuators consisted of the mass flow controllers for both the trimethylgallium (TMG) and trimethylaluminum sources. The spectroscopic ellipsometer was used for both composition and growth rate measurement. However, the controller performance was not examined with any post-growth tests such as X-ray diffraction or photoluminescence. Spectroscopic ellipsometry techniques have also been used for closed loop control of MOCVD growth of HgCdTe (mercury cadmium telluride), a II–VI material system [3]. A proportional controller was used to regulate the flow rate of dimethylcadmium. The composition (x of $Hg_{(1-x)}Cd_xTe$), was measured by an ellipsometer, and the system showed good temperature disturbance rejection. Again post-growth analysis was not reported. Simulation studies have also addressed closed loop control of TMI concentration, using proper orthogonal decomposition (POD) methods in high pressure reactors [4].

In related work [5], trimethylindium (TMI) disturbances were identified and compensated for by using an ultrasonic concentration monitor, and evaluated by post-growth X-ray diffraction analysis. This work was used as an example for the feedforward TMG control system described in Section IV. Significant improvement in composition and thickness regulation was demonstrated via post-growth X-ray diffraction [6]. This paper also summarizes the results in [7], where an ultraviolet (UV) absorption sensor was developed for feedback control of GaInAs growth.

The major contributions of the work reported here are: the development of a control relevant model; the characterization and identification of process disturbances; and the demonstration of the effectiveness of closed-loop control via device growth and a posteriori measurement. The actual control design is not a difficult part of the procedure. Sensor development and disturbance characterization—on a time scale commensurate with control for an individual growth run—are the more significant aspects. This contrasts with run-to-run

© 2001 IEEE. Personal use of this material is permitted. Permission from IEEE must be obtained for all other uses, in any current or future media, including reprinting/republishing this material for advertising or promotional purposes, creating new collective works, for resale or redistribution to servers or lists, or reuse of any copyrighted component of this work in other works.

control methods which are useful in compensating for slower time scale drifts. To our knowledge, this is the first work demonstrating active control using UV absorption sensing for feedback.

The paper is organized as follows. Section II describes the MOCVD process. The control performance goals are defined for this application in Section III. Two control strategies are described. The first is an upstream feedforward approach, outlined in Section IV. This section describes work that was developed in greater detail in [6], and is presented here for completeness. The second control approach uses a UV sensor for feedback control. The sensor is described in detail in Section V, the control model is developed in Section VI, and the control design is covered in Section VII. The closed-loop growth results are presented in Section VIII, and summarized in the conclusions given in Section IX.

II. MOCVD TECHNOLOGY

Figure 1 is a schematic overview of our MOCVD gas delivery system for one source. Each source element is transported as a vapor phase metalorganic and mixed in a very low dead-zone volume manifold, before being injected into the growth chamber where the source elements thermally decompose to form single crystal layers. A low dead-zone manifold does not have a stored gas volume and therefore minimizes the transport delay between the actuation and the growth chamber.

The column III and the column V organic source materials used in this work include tertiarybutylarsine (TBA), tertiarybutylphosphine (TBP), trimethylgallium (TMG) and trimethylindium (TMI). They are stored in a solid or liquid phase in temperature and pressure controlled source vessels (bubblers) and transported by bubbling hydrogen gas through the source. This has significant safety advantages over the more common gaseous sources but introduces additional disturbances due to gas bubbler dynamics. The temperature and pressure control provides a constant evaporation rate from the precursor chemical, and allows for repeatable mixing of the source vapor and the hydrogen carrier.

The source concentration is also regulated by a set of mass flow controllers (MFCs). The input MFC and dilution MFC set the hydrogen flow rate entering the bubbler and the hydrogen/component dilution factor, respectively. An injection flow controller, located prior to the injection manifold, controls the amount of the vapor mixture introduced into the reaction chamber and is used as our primary control actuation. The injection flow is always set to a smaller value than the input plus dilution flow in order that the bubbler pressure can be controlled via the bubbler pressure control valve (PCV).

The system is equipped with an ultrasonic concentration sensor which is used for feedforward bubbler concentration disturbance rejection. We have designed and built a UV absorption monitor which is capable of measuring the concentration of a single source gas immediately prior to deposition, and is used here for feedback control [7]. The concentration and absorption sensor systems are discussed further in Sections IV and V, respectively.

The susceptor (growth surface) is maintained under tight temperature control between 500 and 750° C . In this range the growth rate is determined primarily by the component mass transport, rather than the reaction kinetics, and we can make the following assumptions: the incorporation of column III atoms is dependent solely on the amount of column III source vapor introduced into the reactor cell; column III precursor molecules are fully decomposed; column III precursor partial pressure goes to zero at the interface; and column V source vapor is supplied in excess and does not impact growth rate or alloy composition of ternary compounds having two group III constituents [8, p. 115].

Under these assumptions the growth rate is a linear function of the column III source delivery rate. Using TMG and TMI as column III examples, the growth rate, r_g, is given by,

$$r_g = k_m f_{\text{III}} = k_m(a f_{TMG} + b f_{TMI}), \quad (1)$$

where k_m is the mass-transport coefficient, f_{III} is the molar or pure component flow (PCF) rate of group III source, and a, b are the gallium and indium sticking coefficients, respectively. Under the growth conditions considered here these coefficients do not have significant temperature dependence [9], [8]. The solid composition is a ratio of the column III growth rates,

$$x = \frac{k_1 f_{TMI}}{k_1 f_{TMI} + k_2 f_{TMG}} = \frac{f_{TMI}}{f_{TMI} + k f_{TMG}}, \quad (2)$$

where x is the mole ratio as in $Ga_{(1-x)}In_xAs$ and $k=k_1/k_2$ is a growth coefficient. These two relationships are the foundation for growth recipe design. In order to obtain the desired composition and thickness, the gas handling system must deliver the appropriate pure component flows of the column III reactants. For typical open loop operation, the actuator set points are selected based on these relationships.

III. MOTIVATION FOR CONTROL

MOCVD recipes are typically specified in terms of PCF—which is the product of precursor concentration in the carrier gas and mass flow rate—and switching times for the various sources. Pre-growth calibration is used to set up the mass and pressure controllers to achieve the desired PCF for each source. From this point, the recipe is followed in an open-loop fashion. Concentration disturbances [5], [6] can can perturb both the thickness and concentration of the device layers.

Figure 2 shows the concentration of TMG, as measured by the ultrasonic concentration monitor during a normal growth run. Comparison with the hydrogen only case, in which the bubbler was bypassed, illustrates the sensor noise characteristics and highlights a significant bubbler disturbance in the 0.01 – 0.1 Hz. frequency range. The bubbler disturbance is capable of corrupting the growth of even a single layer and the 0.4% tolerance band shown is a typical disturbance tolerance bound. Potential sources of this disturbance are: thermal dynamics of the source bath (held at -10° C); and the disturbances introduced by multiple MFC and pressure actuators.

The two control schemes studied are depicted in Figure 3. The first control scheme is a feedforward disturbance rejection controller on the TMG gas delivery system. This is described in more detail in [6] and is summarized in Section IV. The control actuator is the TMG injection MFC and the control sensor is the ultrasonic concentration monitor. The

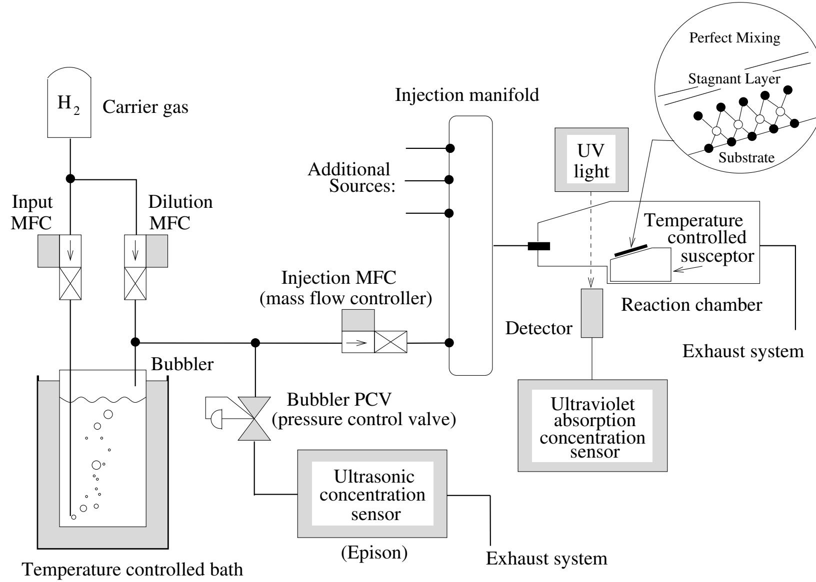

Fig. 1. Simplified overview of the MOCVD process for one source (the sensors and actuators are highlighted)

performance goal was to regulate the pure component flow in the presence of the TMG bubbler disturbances in order to improve the composition and thickness precision. The controller performance was evaluated by growing a GaInAs/InP superlattice structure under both compensated and uncompensated conditions. The second control scheme is a feedback control scheme, (discussed further in Sections V through VIII) using a UV absorption sensor for concentration measurements and controlling the injection MFC for the TMI source. In this case, TMI was chosen because it has more variability than other column III sources. It is stored in a solid state with a lower vapor pressure than the other sources, which are stored in liquid states [5], [10]. The controller objective in this case was the rejection of the higher frequency disturbances in the pure component flow that originate from the TMI bubbler. This complements the feedforward scheme by rejecting the higher frequency disturbances.

The configuration of our reactor prevented a direct sample measurement via reflectance methods such as ellipsometry, and this motivated the selection of a UV absorption sensor.

IV. Upstream Feedforward Control System

The primary controller objective is to use the ultrasonic concentration monitor to reject the disturbances to the bubbler concentration. This monitor has a bandwidth of approximately 0.1 Hz and is therefore effective for the rejection of the 0.01-0.1 Hz low frequency disturbances.

Actuation is accomplished via the injection MFC just prior to the manifold, as shown in Figure 3. A simple static nonlinear inversion is used to generate the controller actuation, the mass flow rate setpoint F_{set}, via $F_{set} = f_{target}/C_{epi}$, where C_{epi} is the ultrasonic concentration measurement and f_{target} is the desired growth recipe PCF. The control structure is illustrated in Figure 4. As shown, this static inversion is implemented in a feed forward fashion to reject the bubbler concentration disturbance (C_{dist}) and thereby obtain the desired pure component flow rate (f_{target}). In the actual implementation, the ultrasonic concentration sensor signal was filtered using a 0.1 Hz, 2-pole Butterworth filter to reduce the noise and also prevent the controller from responding to erroneous concentration monitor signals. See [7] for further details. for further details.

To evaluate this system the multi-layer InP/GaInAs device illustrated in Figure 5 was grown. Growths were run with and without the controller in action, and the results evaluated by post-growth X-ray diffraction analysis. The test device consisted of alternating layers of InP (indium phosphide) and GaInAs (gallium indium arsenide), which exhibited the behavior of a 4-period GaInAs/InP (3000 Å/200 Å) superlattice structure. The desired layer thicknesses and growth times are shown in the figure. The multi layer feature of the structure allows the investigation of composition at defined stages of growth. The GaInAs layer thickness was chosen to give a sufficiently strong X-ray diffraction signal from each layer, without significantly attenuating the signal from lower layers. The controller regulates only the pure component flow of TMG, so even under feed forward control, disturbances in the other sources can corrupt the composition of the alloy, in particular the remaining column III source, TMI.

The layer-to-layer solid composition and thickness was investigated with a double-crystal X-ray diffractometer using Cu Kα_1 radiation and (004) reflection. This involves rocking the illuminated sample to vary the incidence angle and measuring the diffracted X-ray count. Constructive and destructive interference can be observed as a function of rocking angle. If the device grown was a ($Ga_xIn_{1-x}As$) layer on an InP substrate, one would expect two peaks in the rocking curve, the first for the InP lattice and the second for the GaInAs lattice. A full-width, half-maximum (FWHM) parameter of

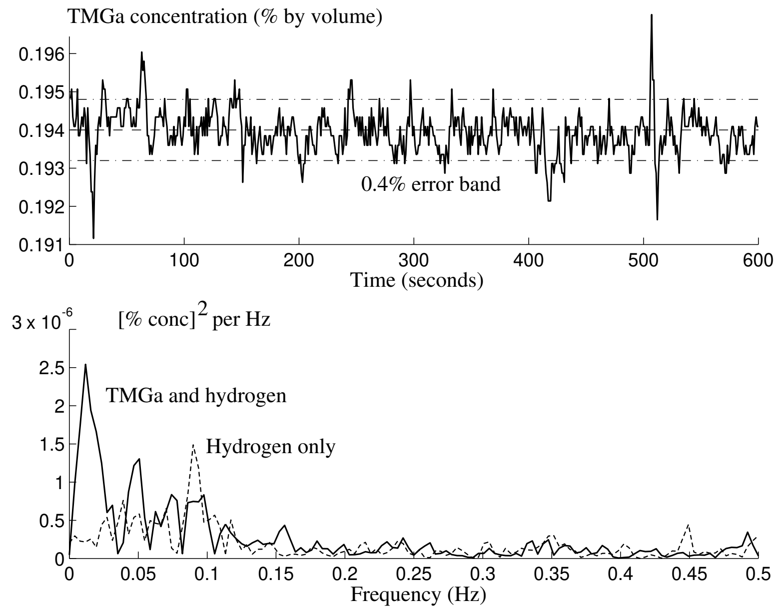

Fig. 2. TMG concentration variation during growth

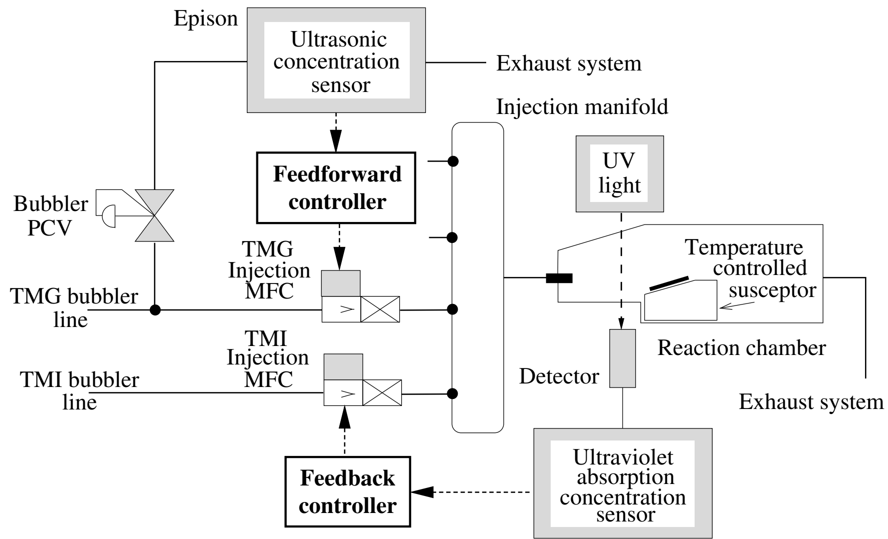

Fig. 3. Feedforward and feedback control schemes

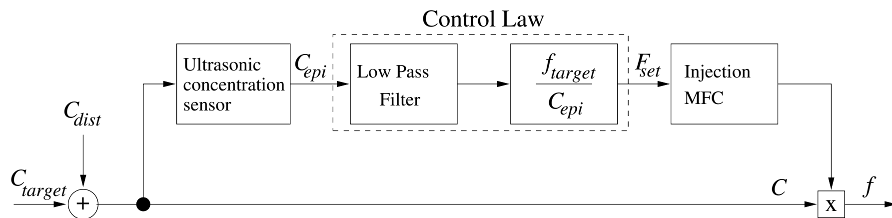

Fig. 4. Block diagram of the feed forward control system used to reject the bubbler disturbance

Growth time (sec)		GaInAs layer
214	3000 Å GaInAs	Layer 5
74	200 Å InP	
214	3000 Å GaInAs	Layer 4
74	200 Å InP	
214	3000 Å GaInAs	Layer 3
74	200 Å InP	
214	3000 Å GaInAs	Layer 2
74	200 Å InP	
214	3000 Å GaInAs	Layer 1
115	1000 Å InP	
	InP Substrate	

Fig. 5. Feedforward demonstration device structure

the GaInAs layer peak is used to characterize the quality of the substrate or growth layer crystal lattice. A smaller width implies a tighter composition precision throughout that layer. The relative angle between the substrate and layer peaks can be used to determine the lattice mismatch, which can then be related to the desired composition to verify the alloy molar composition breakdown. In multi-layered structures (as shown in Figure 5) higher-order constructive interference patterns generated by the lower layers show up as satellite peaks on the rocking curve. In superlattice structures, the presence of satellite peaks is used as a measure of high crystalline quality where both the thickness and composition of the periods are precisely repeated.

Figure 6 shows the rocking curves for uncompensated and compensated growths. The FWHM of the main GaInAs peak is narrower in the compensated case (120 arc sec. vs. 200 arc sec.) indicating tighter control of the solid concentration. Standard analysis software estimates and deconvolves the satellite peaks before estimating the FWHM. The primary feature in the compensated results, (Figure 6(b)), which is evidence of an improved growth, is the presence of at least eight pairs of well-defined satellite peaks. Satellite peaks occur in pairs, one to either side of the main peak. The GaInAs satellite peaks to the right of the GaInAs main peak are easily distinguished in the figure. The GaInAs satellite peaks to the left of the GaInAs main peak are obscured by the InP satellite peaks and the InP main peak. The satellite peaks in the compensated case result from higher order constructive interference with the lower layers and indicate consistency in both thickness and composition between the layers. The compensated curve is compared to an ideal material simulation. The qualitative match between the simulation of the nominal device structure and the actual measurement further confirms the ability of the controller to improve reproducibility from layer to layer, a major requirement in superlattice growth.

V. Ultraviolet Absorption Monitor

The feedback control scheme is based on a UV absorption monitor, the principles of which we now describe. Beer's law can be used to predict the UV absorption, A, of the group IIIb and group Vb alkyl compounds used in MOCVD growth, as follows:

$$A = \log_{10} \frac{I_o}{I} = \varepsilon(\lambda) L C, \qquad (3)$$

where I_o is the intensity of the incoming monochromatic light, and I is the intensity of the light exiting the sample. The molar absorption or extinction coefficient, ε, is a parameter that describes the probability of absorption at a single wavelength. The optical path length is L, and C is the molar concentration, which is the variable we wish to measure. In a non-interacting mixture the absorbances add and the concentrations within an n gas mixture can be determined—subject to sufficient variation in $\varepsilon(\lambda)$ for each gas—by using n different wavelengths and applying numerical regression techniques. The work described here uses a single wavelength (211 nm) and measures only the concentration of TMI.

Numerous research groups have developed UV absorption monitoring systems to study MOCVD growth, including [11], [12], [13], [14], [15], [16], [17]. The work in [18] reports evidence of bubbler concentration variations and suggest the use of UV spectroscopy to control the precursor concentration and improve the MOCVD fabrication of high-temperature superconducting thin films. Further work in [10] claims to have used UV spectroscopy to monitor and control the growth of InSb films. Although no details of the control work were given, it was confirmed that the cited compensation was performed via manual adjustments, based on a "human-in-the-loop" feedback system using in situ UV absorbance measurement of each reactant [19], [20]. No results comparing open and closed loop results were presented. The results presented here are a subset of those found in [7], which describes an active control growth demonstration using ultraviolet absorption sensing for the feedback signal.

The UV absorption monitor hardware configuration is illustrated in Figure 7. The physical configuration was constrained by the high temperatures in the vicinity of the reactor deck. Consequently, there were several optical components required to steer the light into the reactor. Sensor components located on the reactor deck include only the mirror and three lenses, which are indicated in Figure 7. The lamp, chopper and electronic equipment are placed on the roof of the reactor deck. The monochromator and PMT were cantilevered behind the back panel of the reactor deck. The optical path length within the reaction chamber is 6.35 cm.

The UV light source is a 30 Watt ozone free deuterium lamp, with the peak spectral irradiance in the range 200 to 300 nm. A monochromator optically filters the polychromatic light to a wavelength of 211 nm with a 6 nm resolution and the photomultiplier tube (PMT) converts the light intensity to an electrical signal. A mechanical chopper/lock-in amplifier system—operating at a 166 Hz chopper frequency—modulates the source light and amplifier synchronously to reject ambient light level variations. The output of the lock-in amplifier

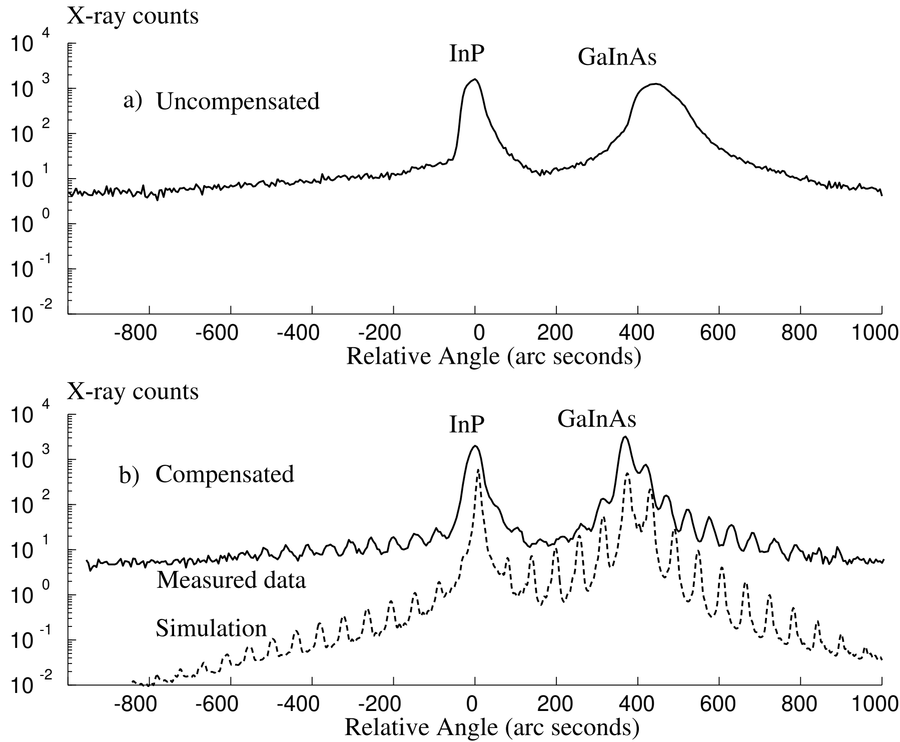

Fig. 6. X-ray diffraction rocking curves of the uncompensated and compensated growths. At least eight satellite peaks are observed on the right hand side of the GaInAs peak. Those to the left are obscured by the InP peak satellites.

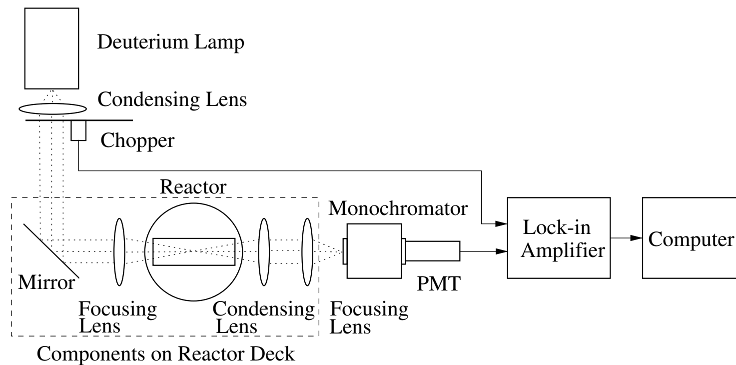

Fig. 7. UV monitor configuration

is sampled at 50 Hz. by a computer running the LabView software instrumentation package.

Figure 8 shows a typical UV transmission record taken during the growth of an InP/GaInAs(P) device. Photolysis—the breakdown of gas components due to the UV light energy—causes slow material deposition on the chamber walls in the optical path and this can be seen in the initial region of the time history. This means that the UV monitor gives only a relative absorption measurement and cannot be used to correct slow concentration drift. The photolysis problem can be avoided by specialized reactor designs [13], but this is beyond the scope of the current work.

VI. Downstream System Model for Control

A block diagram of the MOCVD process model and closed-loop compensator is shown in Figure 9. The MFC setpoint, F_{set}, is again determined by the required growth recipe PCF. System disturbances include concentration (C_{dist}), absorption drift (A_{drift}) due to photolysis, and absorption measurement noise (A_{noise}). Recall that an absolute measure of concentration is not available due to the photolysis drift. In terms of controller design, a differential measure of concentration (no dc component) is equivalent to a differential measure of absorbance, as long as the model gain from PCF to absorbance is correct. As a result, the plant model output and controller input is specified in terms of absorbance.

A linear model of the MFC was estimated by subspace

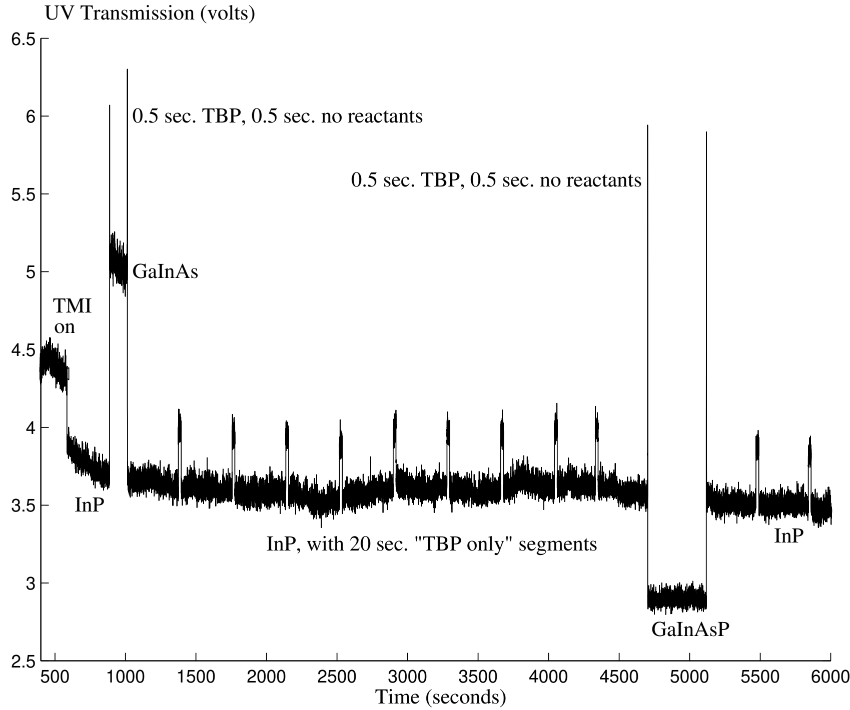

Fig. 8. UV transmission: InP/GaInAs(P) at 211 nm

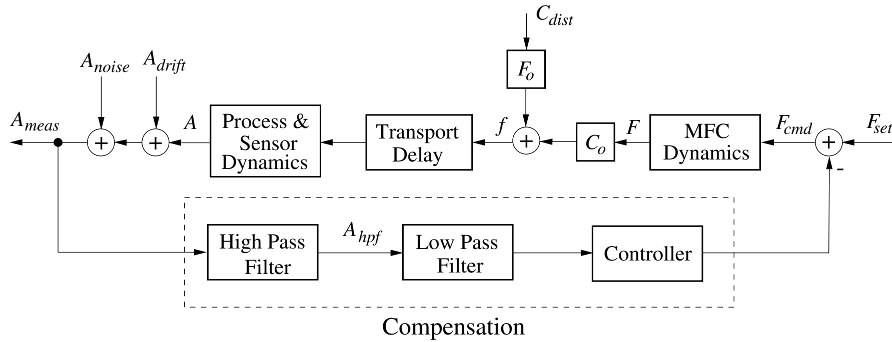

Fig. 9. Schematic model of the closed loop system, illustrating the component parts of the plant model and controller

based time domain system identification techniques [21]. The nonlinear PCF relationship, $f = CF$, was linearized and the nominal concentration and mass flow values are shown as C_0 and F_0 respectively in Figure 9. The process delay was estimated, by recording switching events, to be 0.4 seconds. The delay was modeled with a first order Padé approximation. Subspace identification was also used to estimate a linear model for the remaining process and sensor dynamics. These dynamics include species mixing and the lock-in amplifier filters. The absorption measurement, A_{meas}, was calculated from real-time measurements of intensity I, and a recent estimate of I_o, using Beer's Law (Equation 3). The open-loop frequency response of the entire linear plant model, from the TMI MFC set point input, F_{cmd}, to the measured absorbance output, A_{meas}, is illustrated in Figure 10. The absorption magnitude units are arbitrary because the quantity is unitless. The DC gain of the plant model is 7.91×10^{-5} absorb. units sccm^{-1}. As shown, the plant model magnitude starts to roll off quite rapidly after 0.4 Hz. The phase loss at 0.1 Hz is -46.47 degrees. The phase loss is attributed to both the UV sensor dynamics, including the lock-in amplifier, and the transport delay. The control system was designed using classical methods, hence the frequency response of the plant model was the basis for the design.

VII. Downstream Feedback Control Design

The controller structure illustrated in Figure 9 explicitly depicts the filtering required for the absorption measurement. Photolysis induced drift corrupts the measurement and the high pass filter removes the low frequency component of the signal. The controller filters limit the measured absorption to the range 0.006 to 1.0 Hz. Note that the controller output is summed

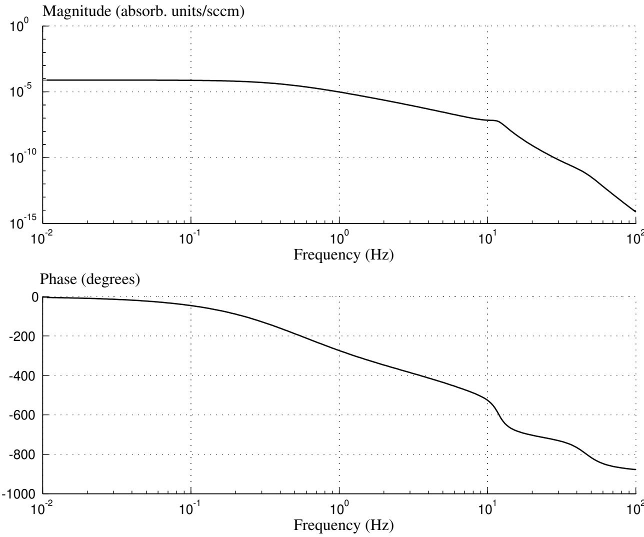

Fig. 10. Estimated open-loop frequency response of the plant from the TMI MFC setpoint input, F_{cmd}, to the measured absorbance output, A_{meas}.

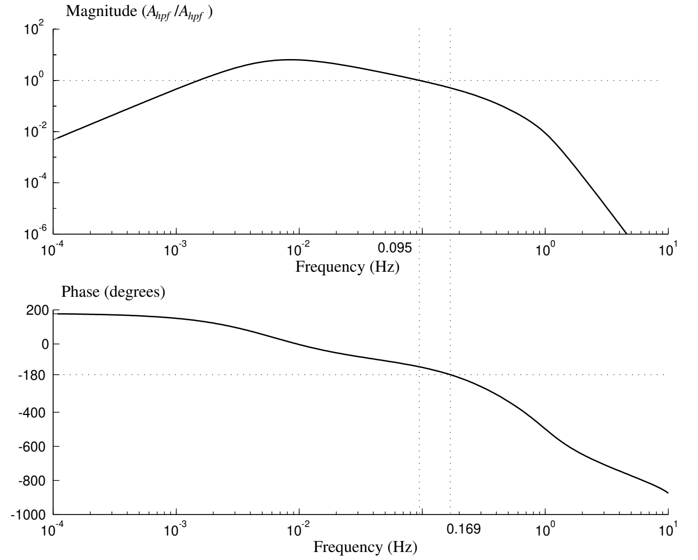

Fig. 11. Frequency response of the loop transfer function. The frequencies for the gain and phase margins are marked.

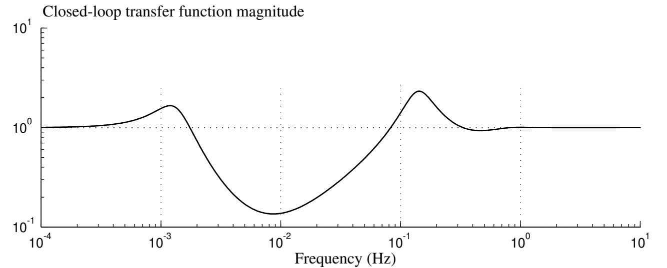

Fig. 12. Closed-loop C_{dist} to A transfer function.

with the MFC setpoint command which provides the desired DC control value.

The closed-loop design objectives for $C(s)$ were: minimizing the C_{dist} to A transfer function in the range 0.009 to 0.02 Hz.; giving zero DC response for the A_{drift} to A transfer function; minimizing the A_{noise} to A transfer function at high frequencies; and normalizing the F_{set} to A transfer function at DC to obtain the desired PCF. Recall that A is directly proportional to the concentration of TMI. Note that the frequency range where disturbance rejection is required is more than an order of magnitude lower than the dominant process time constant.

Classical loopshaping techniques are adequate for a control design in this case, and the performance objectives were met with a high gain lag controller, with a pole at -0.005 Hz,

$$C(s) = \frac{2528.4}{31.8s+1}. \tag{4}$$

The controller pole location is a compromise between maximizing the gain over the performance bandwidth and providing sufficient gain roll-off before the process delays degrade the phase margin.

The frequency response of the loop transfer function is illustrated in Figure 11. The final design had a phase margin is 46 degrees, at the cross over frequency of 0.095 Hz, and a gain margin of 5.89 db at 0.169 Hz. Note that at low frequencies the system is gain stabilized. As shown in Figure 11, the disturbance rejection performance, indicated by the magnitude of the open loop transfer function at the disturbance frequency, could have been increased at the expense of the stability margins.

Figure 12 shows the closed-loop C_{dist} to A transfer function achieved by the design, and shows performance improvement in the 0.002 to 0.7 Hz range. This corresponds to rejecting disturbances which would normally corrupt a typical 1000 Å layer at a typical growth rate of 10 Å/sec.

The closed loop frequency response from A_{drift} and A_{noise} to A can be found in Figure 13. The key features of this plot include the low frequency rejection of the photolysis drift and the high frequency attenuation of absorbance measurement noise. The drift attenuation ends at approximately 0.004 Hz and the noise attenuation is approximately 1×10^{-7} at 10 Hz.

VIII. Closed-loop Growth Results

The UV sensor based feedback was tested separately from the ultrasonic feedforward control, and required a device growth demonstration that would show the mid frequency range disturbance rejection properties. The test device, illustrated in Figure 14, was designed to demonstrate the controller performance and was grown under both open- and closed-loop conditions. The test device consisted of a buffer layer of InP (indium phosphide), and a bulk layer of GaInAs (gallium indium arsenide). The growth times and estimated layer thicknesses are shown in the figure, although the layer thicknesses are not drawn to scale. Control of TMI only occurs in the GaInAs layer. The first 250 seconds of GaInAs deposition are grown under open loop conditions in both the open loop and closed loop test runs. This thick layer was designed for several reasons. First, growth of this layer

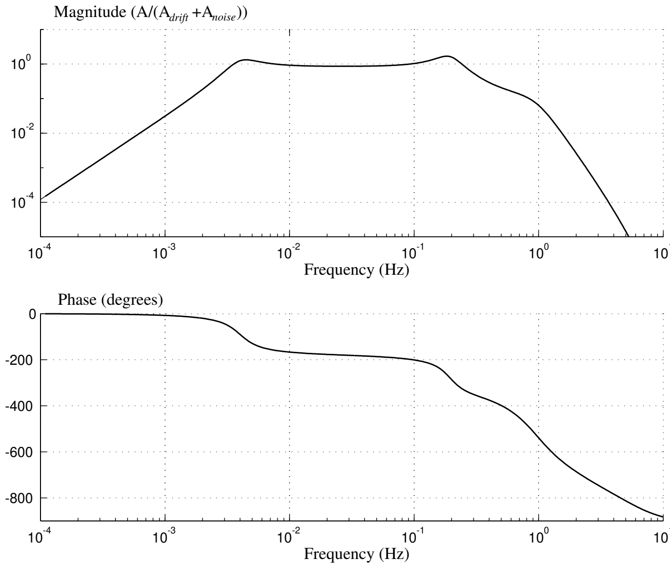

Fig. 13. Frequency response of the closed loop transfer function from the absorbance drift and noise input to the true absorbance output.

Growth time (sec)	Layer	CL Test	OL Test
400	4900 Å GaInAs	CL (dist)	OL (dist)
100	1225 Å GaInAs	CL	OL
250	3062.5 Å GaInAs	OL	OL
300	1710 Å InP		
	InP Substrate		

Fig. 14. Feedback demonstration device structure

provides time for the UV absorption monitor to settle to a steady state condition after responding to the illumination of the growth lamps. Moreover, during this open loop layer, the controller initial conditions are set, and the controller high pass filter reaches a steady state value before the loop is closed. As shown in Figure 14, for the closed-loop test, the loop is closed after the first 250 seconds of GaInAs growth. Before injecting the concentration disturbance, a 100 second layer of GaInAs is grown under closed loop (nominal) conditions, to ensure that the control system has the expected behavior. Then, the concentration disturbance is initiated after 350 seconds of bulk layer GaInAs growth. The concentration disturbance is applied for the remainder of the growth, which consisted of 400 seconds of GaInAs deposition.

The growth of the 4900 Å bulk layer was perturbed by a 0.01 Hz periodic bubbler pressure disturbance, such as might arise from a poorly tuned pressure controller. In the open-loop case this disturbance will generate a period concentration disturbance in the crystal which will give rise to satellite peaks in the X-ray diffraction rocking curve of the resulting device. The closed loop growth should reject the perturbations and not show any evidence of satellite peaks.

Time histories of both closed and open loop signals of interest are compared in the following plots. All time histories begin 150 seconds after the onset of GaInAs growth or in other words 100 seconds before closed loop control is invoked. Figure 15 clearly illustrates that the closed loop system rejected the concentration disturbance, as the open-loop plot (a) displays a measurement of the periodic concentration disturbance, and the closed-loop plot (b) displays only a very small response to the same disturbance type. Other features to note include the transient response of the closed-loop system at time t=100 seconds, when the loop was closed. In addition, both cases show a prominent photolysis drift, as evidenced by the downward ramping UV transmission.

These same data sets were converted into absorbance measurements to compare the performance in terms of the signal driving the controller. The plots, shown in Figure 16, were detrended to remove the photolysis drift and allow direct comparison in the frequency range of interest. The closed-loop disturbance attenuation is clear.

Again, post-growth analysis was performed by X-ray diffraction and the rocking curves are shown in Figure 17. As predicted, the open-loop curve shows significantly greater satellite peaks than the closed-loop case. Simulations were tuned to give the closest match to the rocking curve and then used to estimate the mole ratio disturbance amplitudes in the open- and closed-loop cases as 3.9×10^{-3} and 5.5×10^{-4} respectively. This is almost an order of magnitude improvement in the closed-loop case, confirming the predicted disturbance rejection capabilities illustrated in Figure 12.

Photoluminescence (PL) tests were also used for post-growth analysis and the results are shown in Figure 18. This test measures radiative recombination as a result of single wavelength optical excitation. The closed-loop device peak has a FWHM of 95 nm, compared to 130 nm for the open-loop device, indicating that there is less mole ratio variation in the closed-loop case. Note also that the closed-loop PL peak is three times higher; one hypothesis is that the open-loop device has more dislocations resulting in nonradiative recombination.

IX. Conclusions

Two control schemes have been developed and tested on the MOCVD reactor. An upstream feedforward system, based on ultrasonic concentration sensing, is capable of rejecting low frequency drift and bubbler disturbances. The feedforward scheme is first described in [6] and outlined here for completeness. A downstream feedback system, based on UV absorption sensing, rejects higher frequency disturbances. In both cases the results are demonstrated by post-growth analysis of crystal devices. The two systems operate in complementary frequency ranges and on-going work involves combining the two designs. We are also investigating using multispectral UV analysis to monitor and control multi-gas concentrations within the reactor.

Acknowledgments

The authors appreciate the technical guidance from Nigel Mason at the University of Oxford.

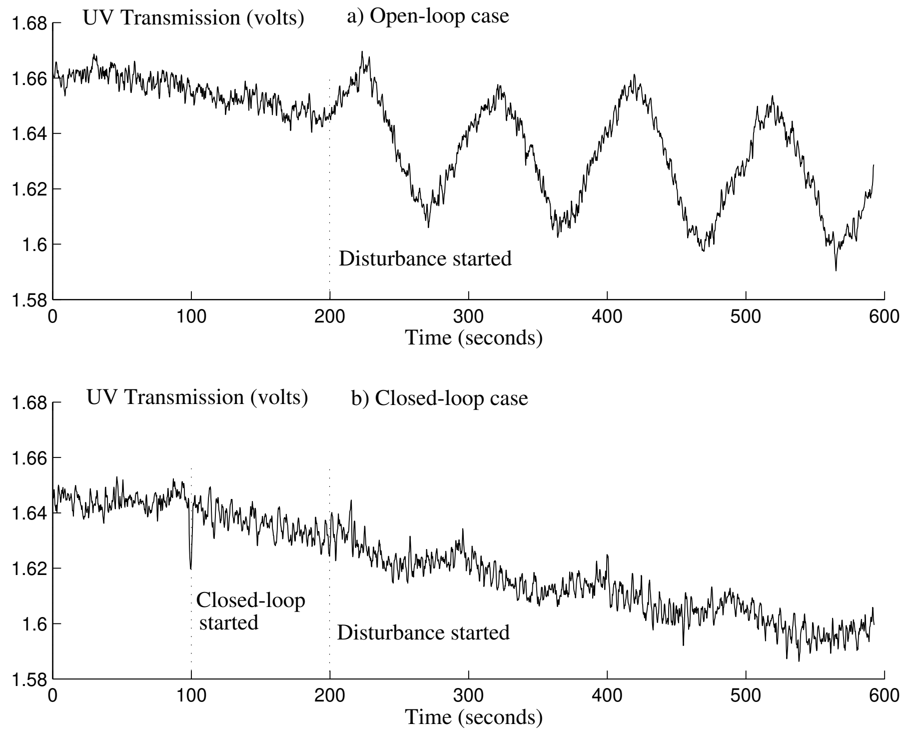

Fig. 15. The (a) open loop and (b) closed loop time histories of the UV transmission intensity in volts.

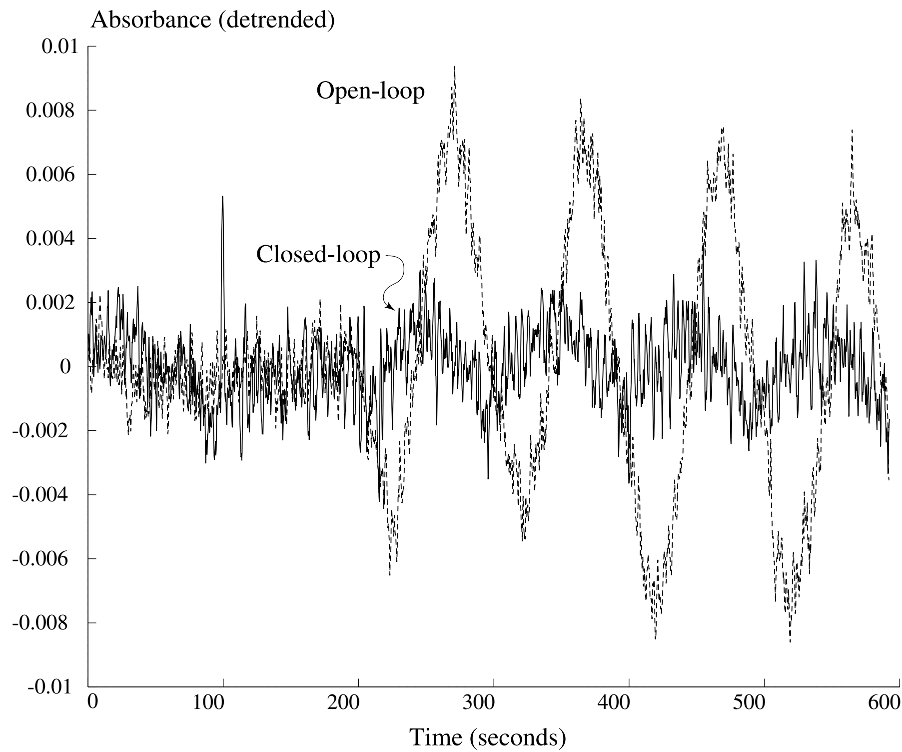

Fig. 16. Absorption measurements (detrended)

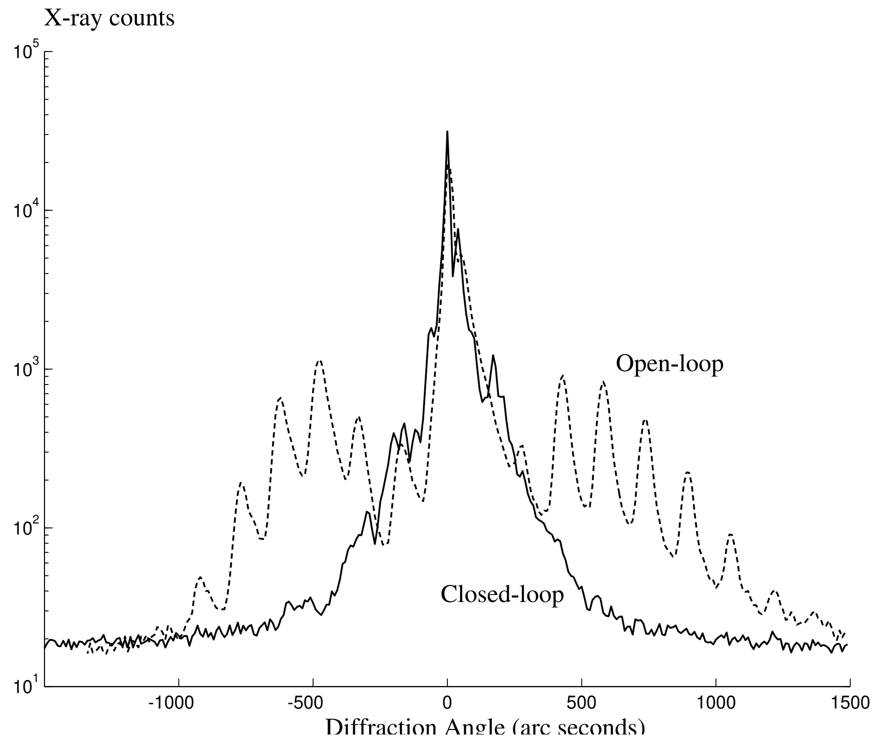

Fig. 17. Post-growth X-ray diffraction analysis

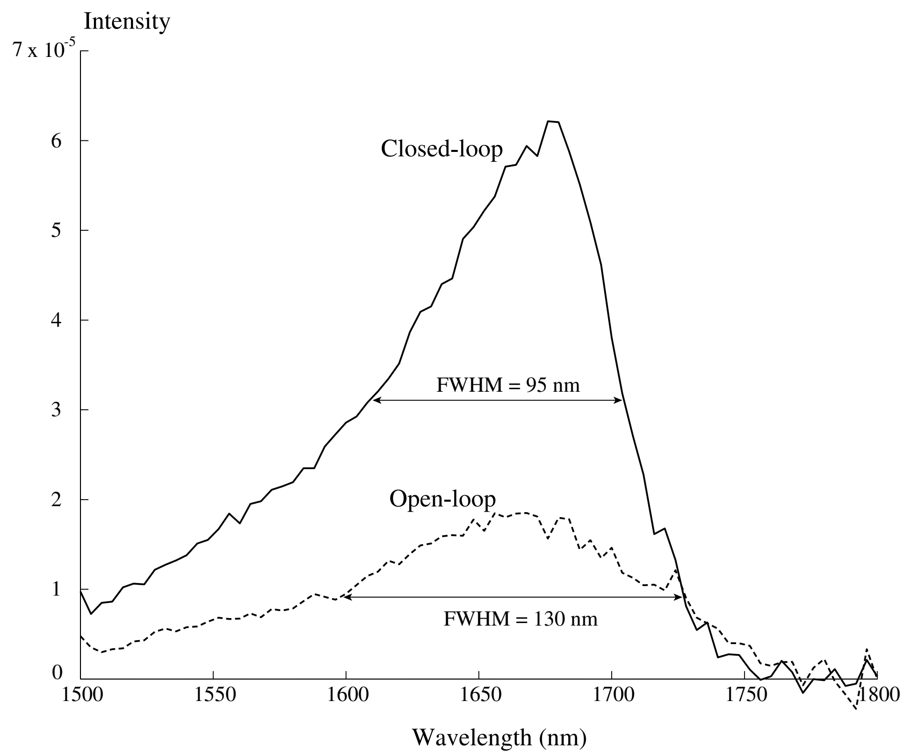

Fig. 18. Post-growth photoluminescence analysis

REFERENCES

[1] D. E. Aspnes, W. E. Quinn, and S. Gregory, "Application of ellipsometry to crystal growth by organometallic molecular beam epitaxy," *Appl. Phys. Lett.*, vol. 56, no. 25, pp. 2569–2571, 1990.

[2] S. C. Warnick and M. A. Dahleh, "Feedback control of MOCVD growth of submicron compound semiconductor films," *IEEE Trans. Control Syst. Tech.*, vol. 6, pp. 62–71, January 1998.

[3] S. Murthy, I. Bhat, B. Johs, S. Pittal, and P. He, "Real-time control of HgCdTe growth by organometallic vapor phase epitaxy using spectroscopic ellipsometry," *J. Elec. Mat.*, vol. 24, no. 9, pp. 1087–91, 1995.

[4] G. Kepler, H. Tran, and H. Banks, "Reduced order model compensator control of species transport in a CVD reactor," Tech. Rep. CRSC–TR99–15, North Carolina State University, 1999.

[5] J. Stagg, J. Christer, E. Thrush, and J. Crawley, "Measurement and control of reagent concentrations in MOCVD reactor using ultrasonics," *J. Crystal Growth*, pp. 98–102, May 1992.

[6] M. S. Gaffney, C. M. Reaves, R. S. Smith, A. L. Holmes, Jr., and S. P. DenBaars, "Control of III-V epitaxy in a metalorganic chemical vapor deposition process: Impact of source flow control on composition and thickness," *J. Crystal Growth*, vol. 167, pp. 8–16, 1996.

[7] M. Gaffney, *Control of a Metalorganic Chemical Vapor Deposition Process for Improved Composition and Thickness Precision in Compound Semiconductors*. PhD thesis, University of California, Santa Barbara, 1998.

[8] G. B. Stringfellow, *Organometallic Vapor-Phase Epitaxy: Theory and Practice*. Academic Press, 1989.

[9] R. Betsch, "Parametric analysis of control parameters in MOCVD," *J. Crystal Growth*, vol. 77, pp. 210–18, September 1986.

[10] D. Ehrlich, G. Higashi, and M. Oprysko, eds., *Photolytic Deposition of InSb Films*, vol. 101, Mater. Res. Soc, 1988.

[11] K. Baucom, K. Killeen, and H. Moffat, "Monitoring of MOCVD reactants by UV absorption," *J. Elec. Mat.*, vol. 24, no. 11, pp. 1703–6, 1995.

[12] R. Karlicek, J. Long, and V. Donnelly, "Thermal decomposition of metalorganic compounds used in the MOCVD of InP," *J. Crystal Growth*, vol. 68, pp. 123–7, 1984.

[13] N. Mason, L. Smith, and P. Walker, "In-situ monitoring of MOVPE alkyl concentrations by UV absorption," in *EW MOVPE VI*, (Gent (Belgium)), IMEC, June 25-28 1995.

[14] G. Booker, M. Daly, P. Klipstein, M. Lakrimi, T. Kuech, J. Li, S. Lyapin, N. Mason, I. Murgatroyd, J. Portal, R. Nicholas, D. Symons, P. Vicente, and P. Walker, "Growth of InAs/GaSb strained layer superlattices by MOVPE III. Use of UV apbsorption to monitor alkyl stability in the reactor," *J. Crystal Growth*, vol. 170, pp. 777–82, 1997.

[15] H. Gilgen, C. Chen, R. Krchnavek, and J. R.M. Osgood, "The physics of ultraviolet photodeposition," in *Laser Processing and Diagnostics* (D. Bauerle, ed.), Chemical Physics 39, pp. 225–33, Springer-Verlag, 1984.

[16] T. Ibuki, A. Hiraya, K. Shobatake, Y. Matsumi, and M. Kawasaki, "He(I) photoelectron spectra and VUV absorption cross sections of $Ga(CH_3)_3$ and $In(CH_3)_3$," *Chemical Physical Letters*, vol. 160, pp. 152–156, August 1989.

[17] H. Itoh, S. Watanabe, and H. Yajama, "Ultraviolet absorption spectra of metalorganic molecules diluted in hydrogen gas," *J. Crystal Growth*, vol. 93, pp. 165–169, 1988.

[18] B. J. Rappoli and W. J. DeSisto, "Gas phase ultraviolet spectroscopy of high-temperature superconductor precursors for chemical vapor deposition processing," *Appl. Phys. Lett.*, vol. 68, pp. 2726–28, May 1996.

[19] R. M. Biefeld, 1998. private communication.

[20] K. Killeen, 1998. private communication.

[21] T. McKelvey, *Identification of State-Space Models from Time and Frequency Data*. PhD thesis, Linköping University, Linköping, Sweden, 1995. Chapter 3.